

# Building High-Throughput Molecular Junctions Using Indented Graphene Point Contacts\*\*

Yang Cao, Shaohua Dong, Song Liu, Li He, Lin Gan, Xiaoming Yu, Michael L. Steigerwald, Xiaosong Wu, Zhongfan Liu, and Xuefeng Guo\*

The ultimate goal of molecular electronics is to understand and control single-molecule devices with robust and identical molecular transport junctions.<sup>[1]</sup> To this end, discrete approaches have been developed for molecular junction fabrication, including break junctions,<sup>[2]</sup> scanning probe techniques,<sup>[3]</sup> sandwich electrodes,<sup>[4]</sup> lithographic methods,<sup>[5]</sup> mercury drop electrodes,<sup>[6]</sup> and others.<sup>[7]</sup> In this study, we describe another efficient method to build molecular electronic devices using point contacts made from graphene as electrodes (Figure 1). Graphene is a remarkable material with extraordinary electronic properties.<sup>[8]</sup> Its high mobility and the ease with which it is doped with either holes or electrons make it useful as a platform for sensors, electrodes in field-effect transistors, and as transparent contacts for photovoltaic devices.<sup>[9]</sup> Herein, we pattern single-layer graphene (SLG) to create point contacts. We create molecular electronic devices by covalently attaching molecules so that they bridge from one graphene point contact to another. This method is related to one that we recently developed to measure the conductivity of individual molecules that are immobilized within gaps in a single-walled carbon nanotube (SWNT) through amide bonds.<sup>[5b]</sup> These SWNT contacts have yielded functional molecular devices that detect molecular conformation transformation, protein/substrate binding, and DNA hybridization.<sup>[10]</sup> This approach is promising, but the connection yield is relatively low (generally 3–5 per cent) and the device-to-device properties vary mainly owing to the variability in the properties of the SWNTs that depend on their chirality and

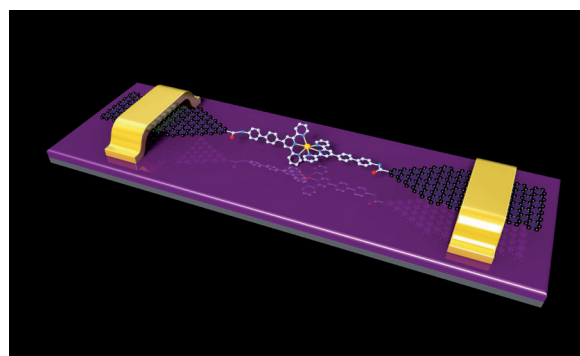


Figure 1. A depiction of single-molecule devices based on graphene point contacts.

diameter. Graphene does not have the inherent variability of SWNTs and could therefore circumvent these problems. We cut SLG precisely using plasma etching through a polymethylmethacrylate (PMMA) mask in which a dash line is lithographically patterned. This process, which we call “dash-line lithography”, yields graphene point contacts by “indenting” the etching into the masked region of the graphene (Figure 2a–c). This etching process produces carboxylic acid-terminated graphene point contact arrays with gaps that are less than or equal to 10 nanometers. These point contacts react with conductive molecules derivatized with amines to form stable molecular devices in high yields (as high as 50 per cent) via amide linkages. These devices can tolerate large changes in the environment. For example, we demonstrate that these devices are able to respond to chemically reactive metal ions.

The process that we developed uses uniform large-area SLGs of high quality by chemical vapor deposition (CVD) on copper foils (details can be found in the Supporting Information).<sup>[11]</sup> Using nondestructive PMMA-mediated transfer and wet-etching techniques, we transferred SLGs onto degenerately doped silicon wafers that were coated by a 300 nm thick layer of thermally grown silicon dioxide (Supporting Information, Figure S1). Raman spectroscopy (Supporting Information, Figure S2d), and high-resolution transmission electron microscopy (Supporting Information, Figure S2e) reveal that the CVD-grown graphene is a single layer. After oxygen plasma etching through a photolithographically patterned resist mask, we obtained graphene sheets that were 250  $\mu\text{m}$  long and 40  $\mu\text{m}$  wide. Then by using a second lithographic process, high-density patterned metallic electrodes (5 nm of Cr followed by 40 nm of Au) separated by 7  $\mu\text{m}$  were deposited onto the SLG sheets through thermal evaporation (Figure 2d). With the metal pads as source (S) and drain (D)

[\*] Y. Cao, S. Dong, S. Liu, L. Gan, Prof. Z. Liu, Prof. X. Guo  
Center for NanoChemistry, Beijing National Laboratory for Molecular Sciences, State Key Laboratory for Structural Chemistry of Unstable and Stable Species, College of Chemistry and Molecular Engineering  
Peking University, Beijing 100871 (P.R. China)  
E-mail: guoxf@pku.edu.cn

L. He, X. Yu, Prof. X. Wu  
State Key Laboratory for Artificial Microstructure and Mesoscopic Physics, Peking University (P.R. China)  
Dr. M. L. Steigerwald  
Department of Chemistry and the Columbia University Center for Electronics of Molecular Nanostructures, Columbia University (USA)

[\*\*] We thank Colin Nuckolls and Philip Kim (Columbia University) for enlightening discussions. We acknowledge primary financial support from MOST (2009CB623703 and 2012CB921404), NSFC (20833001, 51121091, 2112016, 11074007, and 21003002), FANEDD (2007B21), 111 Project (B08001), and BSTSP (2009A01).



Supporting information for this article is available on the WWW under <http://dx.doi.org/10.1002/anie.201205607>.

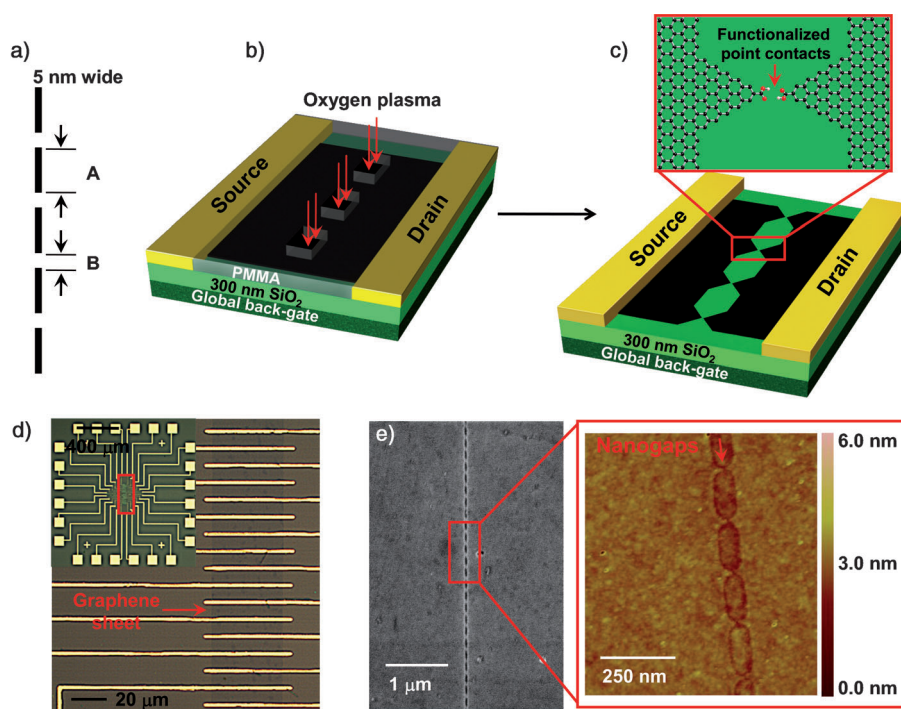


**Figure 2.** Fabrication of indented graphene point contact arrays. a) A DesignCAD file with a 5 nm-width dash line (A, 150 nm; B, 40 nm) used for the cutting process. b) Precise cutting of graphene sheets by oxygen plasma through an indented PMMA window defined by electron-beam lithography. c) Indented graphene point contacts formed by oxidative cutting were functionalized by carboxylic acid end groups and separated by as little as a few nanometers. d) An optical image of integrated graphene FETs located in the center of each pattern. Inset shows the optical image of a whole pattern. e) SEM and AFM images of a representative indented graphene point contact array. Inset: the height profile of the SLG (SLG thickness, ca. 0.7 nm).

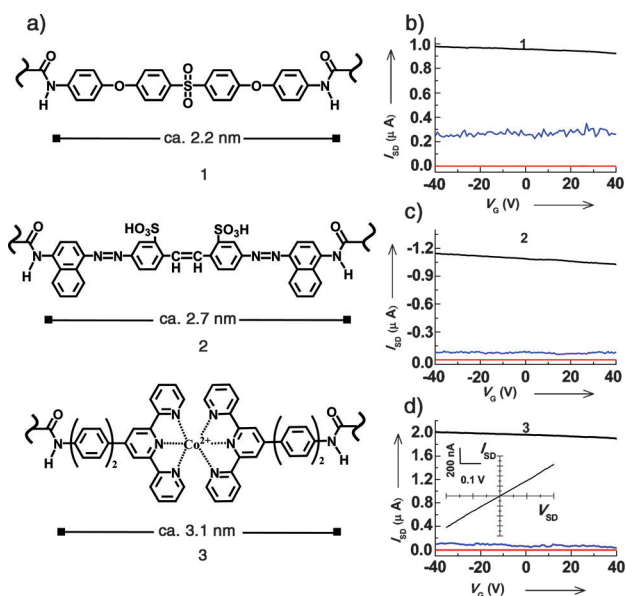
contacts and the silicon substrate as a back gate (G), the graphene devices can be electrically tested, and we find an average sheet resistance of about 0.7–10 k $\Omega$ .

Figure 2a–c illustrates the new method designed to create uniform graphene point contact arrays separated by a few nanometers. We designed a DesignCAD file with a 5 nm-width dash line (A exposed to electron beam (e-beam) separated by B; Figure 2a) to open an indented window in a spin-cast layer of PMMA by using ultrahigh-resolution electron-beam lithography. The graphene sheet was then locally cut through the open window by oxygen plasma ion etching (15 Pa, 30 W RF power, 15 s exposure). By exploiting the gradual etching and undercutting of the PMMA, we achieved narrow gaps between indented graphene point contacts. In addition to the lithographic and etching conditions, the A and B parameters shown in Figure 2a are also crucial. We systematically explored the influences of values A and B on device fabrications (details can be found in the Supporting Information, Figure S4–S7). On the basis of these investigations, given the scattering of the electron beam and the intrinsically limited resolution of the electron-beam writer, we finally fixed A at 150 nm and B at 40 nm for the following device fabrication and molecular connection.

This dash-line lithography proves efficient to create molecular-scale gap arrays with carboxylic acid end-group functionality. Figure 2e shows the scanning electron microscope (SEM) image over large areas of a representative

graphene sheet that was completely cut to give indented point contacts (a total of about 210 pairs). The gaps are too small to be seen in SEM, but it can be located and directly imaged with atomic force microscope (AFM). The relatively large size of the AFM tip makes it difficult to determine with precision how small the gaps are. Considering the imaging convolution of the AFM tip, we estimate the statistical size range of the typical gap arrays of 1–10 nm for the AFM micrograph in Figure 2e. We hypothesize, on the basis of similar work on SWNTs and the graphene,<sup>[5b,12]</sup> that the oxidation initiates the continuous erosion of graphene from the defects that were either present before etching or were induced by the plasma. Given the strongly oxidizing condition induced by oxygen plasma, we expect a prevalence of carboxylic acid end-groups on the cut edges of SLG sheets. By screening the current–voltage ( $I$ – $V$ ) characteristics of the graphene devices before and after oxidative etching, we identified completely cut graphene transistors, which were directly used for subsequent reconnection.

To demonstrate the efficiency and universality of the contacts developed above, three different molecular wires (1–3, circa 2.2, 2.7, and 3.1 nm in length, respectively) that are terminated with the requisite amine functionality were used (Figure 3a; details can be found in the Supporting Information). We bridged molecular-scale gaps along the cut lines in graphene sheets by amide bond formation. This is done with a pyridine solution containing amines and the carbodiimide dehydrating/activating agent EDCI.<sup>[1c]</sup> Figure 3b–d show the comparison of the  $I$ – $V$  curves of the representative devices reconnected by molecules 1 to 3 before cutting, when cut, and after connection, respectively. The black curves show the S–D current ( $I_{SD}$ ) plotted against the gate voltage ( $V_G$ ) at constant S–D bias voltage ( $V_{SD} = -1$  mV) before cutting. We note that all the devices in Figure 3b–d before cutting exhibit p-type electric field effects with little gate-dependence because the neutrality point ( $I_{NP}$ ) shifted to the more positive value, which is probably due to chemical doping and/or charge transfer induced by etching agents and polymer resists used (iron nitrate and PMMA). The red curves, taken after cutting, show no conductance down to the noise limit of the measurement ( $\leq 100$  fA) owing to the nanogaps. After molecular connection, in all cases we observed the recovery of the original properties, albeit at reduced current values (blue traces in Figure 3b–d). These observations are consistent with our previous cases of rejoining SWNT leads in a similar way, where the gate modulates the nanotube conductance more



**Figure 3.** Reconnection of graphene point contacts by molecules 1–3. a) Molecular bridges (1 to 3) spanning SLG point contacts. b)–d) Device characteristics of the representative devices reconnected by each molecule (b for 1, c for 2, and d for 3) before cutting (black curves,  $V_{SD} = -1$  mV), after cutting (red curves,  $V_{SD} = -50$  mV), and after connection (blue curves,  $V_{SD} = -50$  mV), respectively. Inset: the drain current ( $I_{SD}$ ) as a function of the S-D voltage ( $V_{SD}$ ) of the same device after connection at zero gate bias.

strongly than that of the molecules, which is probably due to the mismatch between the nanogap size (a few nanometers) and the dielectric thickness (ca. 300 nm).<sup>[5b]</sup> To demonstrate the technological reliability, we fabricated many more reconnected devices by each molecule (Supporting Information, Tables S1–S3).

One remarkable advantage of this method is the ability to produce graphene point contact arrays on wafer scale. This allows us to optimize and calibrate the etching process. We define the cutting yield ( $Y_{\text{cutting}}$ ) as the fraction of graphene FETs on a chip that are electrically disconnected after oxygen plasma etching and the connection yield ( $Y_{\text{connection}}$ ) as the fraction of the completely-broken devices that are reconnected after molecular connection, respectively. By keeping other parameters constant, changing the etching time (the key parameter) generates different yields of the cutting. We then investigate the relationships among the cutting yield, the molecular length and the chemical connection yield from about 5000 tested devices (each containing circa 210 graphene point contact pairs). Interestingly, we found that the connection yield has a nonmonotonic dependence on the cutting yield. The evolution of the resulting connection yields as a function of the cutting yields for each molecule is shown in Figure 4a–c. In all cases, the connection yields gradually increased to a peak value at the beginning of the cutting yield increase and then gradually decreased. Such behavior is reasonable because the larger cutting yields generated by using longer etching times produce the statistically bigger gaps. When the dominant gap size at a given cutting yield matches the length of the molecules, this cutting yield gives

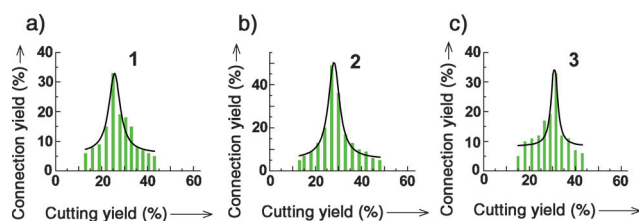


**Figure 4.** Statistical data of the connection yields as a function of the cutting yields for each molecule (a for 1, b for 2, and c for 3). The simulated curves are shown in black.

the maximum connection yield. Under optimized conditions, the maximum connection yield for connection of molecule 1 was found to be about 33%, which corresponds to the cutting yield of 25%. Moreover, for longer molecules (2 and 3), the relatively higher cutting yields are required under identical conditions. For molecule 2, the maximum connection yield is as high as about 50%, which corresponds to the cutting yield of 28%. For molecule 3, the maximum connection yield is 33%, which corresponds to the cutting yield of 31%. These connection values significantly exceed previous studies (Refs. [1c,f] and [1g], and references therein), in which the connection yields were much lower using metal or SWNT leads.

To address the number of junctions that contribute to charge transport, we theoretically calculated the probability of the reconnected devices with  $n$  rejoined junctions ( $G_n$ ) by using the binomial distribution:

$$G_n = \frac{m!}{n!(m-n)!} p^n (1-p)^{m-n} \quad n = 0, 1, 2, \dots, m \quad (1)$$

where  $m$  is the number of graphene point contact pairs (210 in the current case) and  $p$  the probability of connection success for a random junction. Considering the fact that the device becomes conductive even if only one junction is reconnected, the  $Y_{\text{connection}}$  can be expressed by the formula:

$$Y_{\text{connection}} = 1 - G_0 = 1 - \frac{m!}{0!(m-0)!} p^0 (1-p)^m \quad (2)$$

where  $G_0$  is the probability of devices without any reconnected junctions. By taking the  $Y_{\text{connection}}$  values from the experiments, we can obtain the  $p$  value. Then, based on the  $p$  value, the ratios of single-junction or double-junction devices to the overall reconnected devices [ $G_n/(1-G_0)$ ] are calculated (ca. 70% and 24%, respectively) when the connection yield is about 50%. If the connection yield is in the range of 20–30%, the ratio of single-junction devices to the overall reconnected devices is even higher (82–89%). These suggest that in most cases, only one or two junctions contribute to charge transport of the devices. On the basis of this analysis and the data from transport measurements, the device resistance and the molecular conductance can be estimated. For example, the resistance of the device reconnected with the sulfone molecule (1; Figure 3b) increases from about 1.02 k $\Omega$  before cutting ( $V_{SD} = -1$  mV) to  $0.19 \times 10^6 \Omega$  after connection ( $V_{SD} = -50$  mV). Then the molecular conductance for 1 in

this device is calculated to be about  $0.14 e^2/h$ . Similarly, the molecular conductances for **2** and **3** used in Figure 3 c and d, are calculated to be about  $3.97 \times 10^{-2}$  and  $5.32 \times 10^{-2} e^2/h$ , respectively. Statistically, the average molecular conductances for molecules **1–3** are about 0.12,  $4.63 \times 10^{-2}$ , and  $4.85 \times 10^{-2} e^2/h$ , respectively (Supporting Information, Tables S1–S3). One factor that hampers our ability to extract more quantitative information for single molecules is that these conductance values vary from device to device for any given molecule. Realization of atomic level precision in the cutting procedure, and precise control of the molecular conformation on the substrate within the graphene gaps and the contact configuration, are challenges for future studies to overcome.

To rule out potential artifacts from the connection reaction, we carried out systematic control experiments. In one experiment, we used a complex analogous to **3** in which methyl groups replaced the amino terminals. As these molecules cannot react with graphene leads, no reconnection current is expected (Supporting Information, Figure S8). In a second control experiment we used just the single terpyridyl ligands with single amine functionality (**4** in Figure 5 a). Being able to connect covalently to only a single electrode ensures that this species should not conduct. In fact none of the devices showed any detectable current, thus excluding the possibility of molecular aggregates as the agents of conduction. In another experiment, we used 1,12-diaminododecane because it is about the same length as the sulfone molecule **2** but lacks the conjugated backbone. Again, none of the devices showed any detectable current (Supporting Information, Figure S9). This remained the case even when a sulfone was subsequently added; presumably the carboxylic acid sites were already passivated by the alkyl amine. In another experiment, gaps placed in a pyridine solution that contained

the coupling agent but lack any conjugated diamines did not show any electrically connected devices. Furthermore, when we immersed these same gaps in a fresh coupling solution that contains molecule **1**, some of the devices did then become conductive (Supporting Information, Figure S10). Each of these control experiments was performed on about 100 devices to yield a statistically significant null-result.

The contacts made by covalent amide bond formation are quite robust and tolerate broad chemical treatments, thus offering the chance to study the reversibility of coordination reactions (Figure 5). Figure 5 b shows the cycles of decomplexation and complexation with cobalt ions for a device reconnected by molecule **3**. After we immersed the reconnected device in a solution of ethylenediamine tetraacetic acid (EDTA), it became an open circuit (red curve in Figure 5 b). When we introduced  $\text{Co}(\text{OAc})_2$  again, the device nearly returned to its original conductive state (blue curve in Figure 5 b). Moreover, after several cycles of alternate treatments of EDTA and  $\text{Co}(\text{OAc})_2$ , the device still showed good conductance switching (Figure 5 b inset). Control experiments using either the reconnected devices by **1**, which lacks the terpyridyl ligand, or the uncut and partially-cut devices treated with a solution of **3**, were performed under the same conditions. Upon treatments of EDTA and  $\text{Co}(\text{OAc})_2$ , all the devices showed the opposite phenomena to those described above (Supporting Information, Figures S11–S13), which is most likely due to chemical doping or charge transfer induced by chemical adsorbates.<sup>[9c]</sup> These results might provide a potentially valuable method for the fabrication of devices that can recognize individual metal ions.

In summary, we have described a method for fabricating reliable and functional molecular transport junctions in high yield. First, the key advantage of this technique is that the dash-line lithography is able to produce indented molecular-scale graphene point-contact arrays. This methodology circumvents two main challenges facing researchers studying molecular electronic devices: low-yield device fabrication and ill-defined contacts between molecules and electrodes. Our lithographic method allows the chemical preparation of a large number of molecular devices through a well-defined covalent amide bond in high yields (as high as 50 per cent). The molecular devices prepared in this fashion show excellent reproducibility and stability. Second, these molecular junctions allow controllable and diverse functionalization with specific capabilities and detect specific molecular scale activities. In addition to their potential use in building molecular devices, such as switches and sensors, these capabilities can provide an interface between molecular electronics and biological systems.<sup>[13]</sup> Finally, these molecular electronic devices and ability to integrate these hybrid devices into current complementary metal oxide semiconductor (CMOS) technology has the potential to create multifunctional integrated circuits as a significant step towards practical molecular electronics.

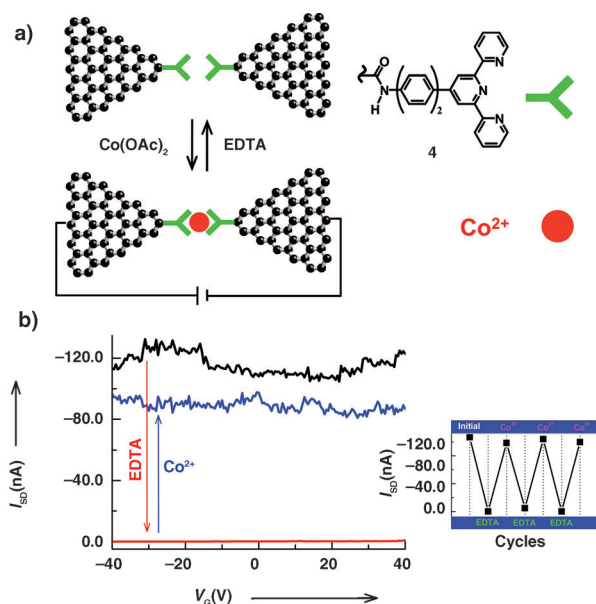


**Figure 5.** a) Strategy for studying the reversibility of coordination reactions. b)  $I_{SD}$  versus  $V_G$  data of a rejoined device by molecule **3** under sequential treatments of EDTA and cobalt ions. Inset: three representative switching cycles for the same device when alternately treated with EDTA and cobalt ions.  $V_{SD} = -50$  mV.

Received: July 15, 2012

Revised: August 28, 2012

Published online: November 4, 2012

Keywords: graphene · lithography · molecular devices

- [1] a) A. Aviram, M. A. Ratner, *Chem. Phys. Lett.* **1974**, *29*, 277–283; b) M. Galperin, M. A. Ratner, A. Nitzan, A. Troisi, *Science* **2008**, *319*, 1056–1060; c) A. K. Feldman, M. L. Steigerwald, X. Guo, C. Nuckolls, *Acc. Chem. Res.* **2008**, *41*, 1731–1741; d) R. M. Metzger, *Chem. Rev.* **2003**, *103*, 3803–3834; e) R. L. McCreery, A. J. Bergren, *Adv. Mater.* **2009**, *21*, 4303–4322; f) T. Li, W. Hu, D. Zhu, *Adv. Mater.* **2010**, *22*, 286–300; g) H. Song, M. A. Reed, T. Lee, *Adv. Mater.* **2011**, *23*, 1583–1608.
- [2] a) M. A. Reed, C. Zhou, C. J. Muller, T. P. Burgin, J. M. Tour, *Science* **1997**, *278*, 252–254; b) J. Park, A. N. Pasupathy, J. I. Goldsmith, C. Chang, Y. Yaish, J. R. Petta, M. Rinkoski, J. P. Sethna, H. D. Abruña, P. L. McEuen, D. C. Ralph, *Nature* **2002**, *417*, 722–725.
- [3] a) Z. J. Donhauser, B. A. Mantooh, K. F. Kelly, L. A. Bum, J. D. Monnell, J. J. Stapleton, D. W. Price, Jr., A. M. Rawlett, D. L. Allara, M. Tour, P. S. Weiss, *Science* **2001**, *292*, 2303–2307; b) X. D. Cui, X. Zarate, O. F. Sankey, T. A. Moore, D. Gust, G. Harris, S. M. Lindsay, *Science* **2001**, *294*, 571–574; c) B. Xu, N. J. Tao, *Science* **2003**, *301*, 1221–1223.
- [4] H. B. Akkerman, P. W. M. Blom, D. M. de Leeuw, B. de Boer, *Nature* **2006**, *441*, 69–72.
- [5] a) L. Qin, S. Park, L. Huang, C. A. Mirkin, *Science* **2005**, *309*, 113–115; b) X. Guo, J. P. Small, J. E. Klare, Y. Wang, M. S. Purewal, I. W. Tam, B. H. Hong, R. Caldwell, L. Huang, S. O'Brien, J. Yan, R. Breslow, S. J. Wind, J. Hone, P. Kim, C. Nuckolls, *Science* **2006**, *311*, 356–359; c) C. W. Marquardt, S. Grunder, A. Błaszczuk, S. Dehm, F. Hennrich, H. von Löhneysen, M. Mayor, R. Krupke, *Nat. Nanotechnol.* **2010**, *5*, 863–867.
- [6] R. E. Holmlin, R. Haag, M. L. Chabinyc, R. F. Ismagilov, A. E. Cohen, A. Terfort, M. A. Rampi, G. M. Whitesides, *J. Am. Chem. Soc.* **2001**, *123*, 5075–5085.
- [7] a) N. B. Zhitenev, H. Meng, Z. Bao, *Phys. Rev. Lett.* **2002**, *88*, 226801–226804; b) S. Kubatkin, A. Danilov, M. Hjort, J. Cornil, J.-L. Brédas, N. Stuhr-Hansen, P. Hedegård, T. Bjørnholm, *Nature* **2003**, *425*, 698–701.
- [8] a) A. K. Geim, K. S. Novoselov, *Nat. Mater.* **2007**, *6*, 183–191; b) A. K. Geim, *Science* **2009**, *324*, 1530–1534.
- [9] a) W. Yang, K. R. Ratinac, S. P. Ringer, P. Thordarson, J. J. Gooding, F. Braet, *Angew. Chem.* **2010**, *122*, 2160–2185; *Angew. Chem. Int. Ed.* **2010**, *49*, 2114–2138; b) Q. Wang, X. Guo, L. Cai, Y. Cao, L. Gan, S. Liu, Z. Wang, H. Zhang, L. Li, *Chem. Sci.* **2011**, *2*, 1860–1864; c) T. O. Wehling, K. S. Novoselov, S. V. Morozov, E. E. Vdovin, M. I. Katsnelson, A. K. Geim, A. I. Lichtenstein, *Nano Lett.* **2008**, *8*, 173–177; d) Y. Cao, M. L. Steigerwald, C. Nuckolls, X. Guo, *Adv. Mater.* **2010**, *22*, 20–32; e) Y. Cao, Z. Wei, S. Liu, Q. Shen, L. Gan, S. Shi, X. Guo, W. Xu, M. L. Steigerwald, Z. Liu, D. Zhu, *Angew. Chem.* **2010**, *122*, 6463–6467; *Angew. Chem. Int. Ed.* **2010**, *49*, 6319–6323; f) W. H. Lee, J. Park, S. H. Sim, S. Lim, K. S. Kim, B. H. Hong, K. Cho, *J. Am. Chem. Soc.* **2011**, *133*, 4447–4454; g) X. Wan, Y. Huang, Y. Chen, *Acc. Chem. Res.* **2012**, *45*, 598–607; h) F. Bonaccorso, Z. Sun, T. Hasan, A. C. Ferrari, *Nat. Photonics* **2010**, *4*, 611–622; i) H. M. Wang, Z. Zheng, Y. Y. Wang, J. J. Qiu, Z. B. Guo, Z. X. Shen, T. Yu, *Appl. Phys. Lett.* **2010**, *96*, 023106; j) K. K. Saha, T. Markussen, K. S. Thygesen, B. K. Nikolić, *Phys. Rev. B* **2011**, *84*, 041412; k) F. Prins, A. Barreiro, J. W. Ruitenbergh, J. S. Seldenthuis, N. Aliaga-Alcalde, L. M. K. Vandersypen, H. S. J. van der Zant, *Nano Lett.* **2011**, *11*, 4607–4611.
- [10] a) A. C. Whalley, M. L. Steigerwald, X. Guo, C. Nuckolls, *J. Am. Chem. Soc.* **2007**, *129*, 12590–12591; b) X. Guo, A. Whalley, J. E. Klare, L. Huang, S. O'Brien, M. L. Steigerwald, C. Nuckolls, *Nano Lett.* **2007**, *7*, 1119–1122; c) X. Guo, A. A. Gorodetsky, J. Hone, J. K. Barton, C. Nuckolls, *Nat. Nanotechnol.* **2008**, *3*, 163–167.
- [11] X. S. Li, W. W. Cai, J. H. An, S. Kim, J. Nah, D. X. Yang, R. Piner, A. Velamakanni, I. Jung, E. Tutuc, S. K. Banerjee, L. Colombo, R. S. Ruoff, *Science* **2009**, *324*, 1312–1314.
- [12] X. Wang, H. Dai, *Nat. Chem.* **2010**, *2*, 661–665.
- [13] a) Y. Choi, I. S. M, P. C. S, S. R. Hunt, B. L. Corso, I. Perez, G. A. Weiss, P. G. Collins, *Science* **2012**, *335*, 319–324; b) S. Liu, X. Y. Zhang, W. X. Luo, Z. X. Wang, X. Guo, M. L. Steigerwald, X. H. Fang, *Angew. Chem.* **2011**, *123*, 2544–2550; *Angew. Chem. Int. Ed.* **2011**, *50*, 2496–2502; c) S. Liu, G. H. Clever, Y. Takezawa, M. Kaneko, K. Tanaka, X. Guo, M. Shionoya, *Angew. Chem.* **2011**, *123*, 9048–9052; *Angew. Chem. Int. Ed.* **2011**, *50*, 8886–8890; d) H. Wang, N. B. Muren, D. Ordinario, A. A. Gorodetsky, J. K. Barton, C. Nuckolls, *Chem. Sci.* **2012**, *3*, 62–65; e) S. Sorgenfrei, C. Y. Chiu, R. L. Gonzalez, Y. J. Yu, P. Kim, C. Nuckolls, K. L. Shepard, *Nat. Nanotechnol.* **2011**, *6*, 125–131.